ADVANCED FUNCTIONAL MATERIALS
www.afm-journal.de

Tunable Volatility of $Ge_2Sb_2Te_5$ in Integrated Photonics

*Nathan Youngblood, Carlos Ríos, Emanuele Gemo, Johannes Feldmann, Zengguang Cheng, Anna Baldycheva, Wolfram HP Pernice, C. David Wright, and Harish Bhaskaran**

The operation of a single class of optical materials in both a volatile and nonvolatile manner is becoming increasingly important in many applications. This is particularly true in the newly emerging field of photonic neuromorphic computing, where it is desirable to have both volatile (short-term transient) and nonvolatile (long-term static) memory operation, for instance, to mimic the behavior of biological neurons and synapses. The search for such materials thus far have focused on phase change materials where typically two different types are required for the two different operational regimes. In this paper, a tunable volatile/nonvolatile response is demonstrated in a photonic phase-change memory cell based on the commonly employed nonvolatile material $Ge_2Sb_2Te_5$ (GST). A time-dependent, multiphysics simulation framework is developed to corroborate the experimental results, allowing us to spatially resolve the recrystallization dynamics within the memory cell. It is then demonstrated that this unique approach to photonic memory enables both data storage with tunable volatility and detection of coincident events between two pulse trains on an integrated chip. Finally, improved efficiency and all-optical routing with controlled volatility are demonstrated in a ring resonator. These crucial results show that volatility is intrinsically tunable in normally nonvolatile GST which can be used in both regimes interchangeably.

1. Introduction

Phase-change materials (PCMs), such as the well-known chalcogenide alloy $Ge_2Sb_2Te_5$ (GST), are best known for their use in the field of data storage,[1,2] although more recent applications include reflective displays[3–5] and tunable optical metasurfaces.[6–8] In the data storage arena they provide the active layer in rewritable optical disks (such as the Blu-ray RE format), and have recently emerged as the basis for a new generation of electrical and photonic memory devices to replace and/or supplement conventional silicon-based memories.[9–12] In these applications, nonvolatile switching of the PCM between its amorphous and crystalline states is exploited to provide binary (or multilevel) storage that is stable for many years.[2,13] However, in new and developing application areas, such as the rapidly growing realm of brain-inspired or neuromorphic computing, it is most desirable for devices to exhibit both volatile (short-term transient) and nonvolatile (long-term static) behavior. Indeed, a single device displaying both these characteristics would potentially have the ability to mimic many of the basic processing and storage operations of the mammalian brain by, for example, providing the short-term plasticity (STP) and long-term potentiation (LTP) observed in synapses,[14–17] as well as delivering essential neuronal features such as the distinctive time-decay of the membrane potential (the "leaky" part of the so-called leaky-integrate-and-fire neuron model).[18,19] Applications in the emerging field of reservoir computing can also be envisaged. In reservoir computing, it is crucial that the dynamics of the reservoir be on the same order as the time scale of the temporal application.[20] Therefore, a device with controllable volatility could act as a volatile, nonlinear element in a reservoir computing network for applications such as speech recognition (where volatility on time scales on the order of tens of milliseconds would be required)[21] or robotic control systems (time scales ranging from tens of milliseconds to several seconds).[22,23]

The ability for combined volatile and nonvolatile operation in a single device could also be used to detect coincident events between multiple inputs. Such coincidence detection is also known to occur in biological neurons, where it is thought to lie at the heart of the processing of information that is embedded in the spatiotemporal structure of neuron spiking patterns (rather than in their mean firing rate).[24] Coincidence detection also has broader significance, for example in the training of neural networks[25] and identifying correlated signals for machine learning applications.[26]

Dr. N. Youngblood, Dr. C. Ríos[+], Dr. Z. Cheng, Prof. H. Bhaskaran
Department of Materials
University of Oxford
Parks Road, Oxford OX1 3PH, UK
E-mail: harish.bhaskaran@materials.ox.ac.uk
E. Gemo, Prof. A. Baldycheva, Prof. C. D. Wright
Department of Engineering
University of Exeter
Exeter EX4 4QF, UK
J. Feldmann, Prof. W. H. P. Pernice
Institute of Physics
University of Muenster
CeNTech II, Heisenbergstr. 11, D-48149 Muenster, Germany
The ORCID identification number(s) for the author(s) of this article can be found under https://doi.org/10.1002/adfm.201807571.
[+]Present address: Department of Materials Science & Engineering, Massachusetts Institute of Technology, MA 02139, USA

DOI: 10.1002/adfm.201807571

Unfortunately, the operation of a single class of optical materials in both a volatile and nonvolatile manner, along with successful integration into a practicable device format, has so far been elusive. Here we demonstrate just such an approach by using PCMs and working in the photonic domain to exploit the potential advantages (in terms of speed, bandwidth, and power consumption) of the silicon photonics "revolution."[27] Although the control of the optical properties of photonic devices has been demonstrated by employing other materials, such as vanadium oxide, metal oxides,[28–32] and even silicon,[33] such control is essentially volatile (e.g., via the thermally induced semiconductor-to-metal phase transition in VO_2). In contrast, we demonstrate here that $Ge_2Sb_2Te_5$, a nonvolatile PCM by design,[2,10,13] also displays a tunable volatility on a photonic waveguide in the presence of a continuous power optical probe. By exploiting this tunable behavior, we demonstrate both nonvolatile multilevel storage and volatile coincidence detection in a single, integrated photonic device.

2. Results

Our photonic device, illustrated in **Figure 1**a, is formed by a 2 µm long and 10 nm thick strip of GST passivated by a 10 nm layer of Indium-Tin-Oxide (ITO) on top of a Si_3N_4 photonic waveguide. Optical WRITE pulses are used to initiate phase transitions while an optical probe is used to continuously monitor the transmission state of the GST. We use the term "optical probe" to denote a variable-power optical signal used to both read and manipulate the state of the material, rather than simply reading out the transmission state without affecting the material itself. Both reading and manipulating the state of GST simultaneously has important consequences as we discuss in more detail below. Light is coupled to the waveguides via grating couplers which are shown in Figure 1b. The center input grating coupler is split into two waveguides which forms the photonic device with GST (right) and a reference arm with no GST (left), allowing us to determine the total transmission of the waveguide and two grating couplers without absorption loss from GST.[9] A false-color SEM image of the GST strip and Si_3N_4 waveguide can be seen in Figure 1c. In order to maximize the interaction between the optical mode and the GST, the sample is annealed at 250 °C for 10 min to crystallize the GST, which increases optical absorption. By applying optical pulses of 50 ns or less, we are able to switch the material between its amorphous (low absorption) and crystalline (high absorption) states in a nonvolatile manner. Finite difference time domain (FDTD) simulations were performed using Lumerical

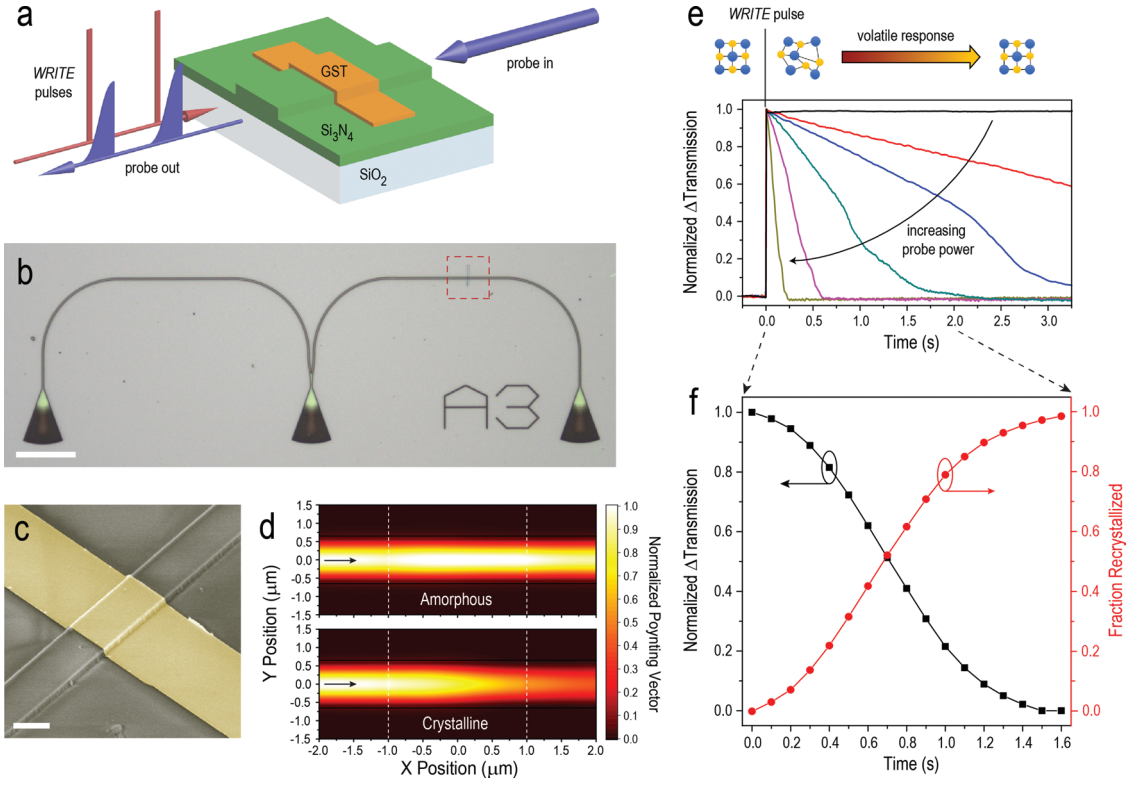

Figure 1. Phase-change photonic device. a) Illustration of device and measurement scheme. Optical WRITE pulses are used to switch the GST to a partial amorphous state while a counter propagating, variable-power optical probe is used to control the recrystallization dynamics. b) Optical image of single device with input grating coupler (center), reference waveguide and output coupler (left), and device waveguide and input/output coupler (right). (Scale bar is 50 µm) c) False-color SEM image of the GST vertical strip overlaying the Si_3N_4 waveguide. (Scale bar is 1 µm) d) FDTD simulations of the power flow from left to right through the region of GST (outlined by white dashed lines) when GST is in both the amorphous and crystalline states. e) Experimental optical transmission of device with increasing optical probe power. At low probe powers (black line), the device remains in the amorphous state for nonvolatile operation, while increasing the probe power causes recrystallization of the GST. f) Simulated optical transmission and crystallization dynamics of the device during volatile operation.

Solutions to calculate the optical transmission through the waveguide when the GST strip is in the amorphous and crystalline states. Figure 1d shows a top-down view of the power flow in the *x*-direction through the waveguide (edges defined by black lines) in the region of the GST strip (edges defined by white, dashed lines), showing a significant reduction in the waveguide transmission when GST is in the crystalline state.

Figure 1e illustrates the observed transmission dynamics of our device when operated in the volatile regime. When an optical WRITE pulse encounters crystalline GST, the pulse is partially absorbed which quickly raises the temperature of the material. If the pulse energy is high enough, a portion of GST will be heated above melting temperature before rapidly quenching below the glass transition temperature, leaving that region in the amorphous state. If we introduce an optical probe to read out the state of the material, some of the optical power is absorbed and converted into heat, depending on the transmission state of the GST strip. For a low-power probe, it is possible to read the transmission state of the GST in a manner that does not influence the physical state of the material (black line in Figure 1e). This is nonvolatile memory which we have demonstrated previously[9,10] and is useful for storing long-term data with a retention time of more than ten years.[2,13] Further details on both stability and multilevel operation are included in Sections S1 and S2 in the Supporting Information. For higher power probes, however, the absorbed optical power can heat the GST near or above the glass transition temperature which causes recrystallization to occur after the initial WRITE pulse as shown in Figure 1e. This memory is volatile with a retention time that is dependent on both the power of the probe and the transmission state of the GST after the WRITE pulse. We note that while the use of constant-power laser irradiation has been previously used to simply crystallize GST in rewritable optical discs,[34] what we present here is an integrated device that allows full optical control of the data retention life time and can be exploited for various uses as discussed later. Figure 1f shows a typical recrystallization curve obtained with custom multiphysics simulations (see Section S3 in the Supporting Information) demonstrating the dynamics of both the optical transmission and the corresponding crystallization fraction (i.e., fraction of GST in the crystalline state).

The amount of GST amorphized by a single WRITE pulse is influenced by the probe power as shown in **Figure 2**a. We define the change in transmission as $\Delta T = (T - T_{min})/T_{min}$, where T_{min} is the transmission of the probe when the device is in the fully crystalline state. The maximum ΔT plotted in Figure 2a is the observed change in transmission occurring after the initial WRITE pulse. In addition to causing recrystallization, increasing the probe power heats the material and increases the absorption of the WRITE pulse through both thermo-optic and electronic effects in GST.[35,36] This is clearly observed in Figure 2a where the maximum change in transmission increases with increasing probe power.

In order to further determine the role of optical probe on the recrystallization dynamics of our device, we fixed the WRITE pulse energy at 485 pJ while varying the probe power. Figure 2b shows the normalized time-dependent transmission of our

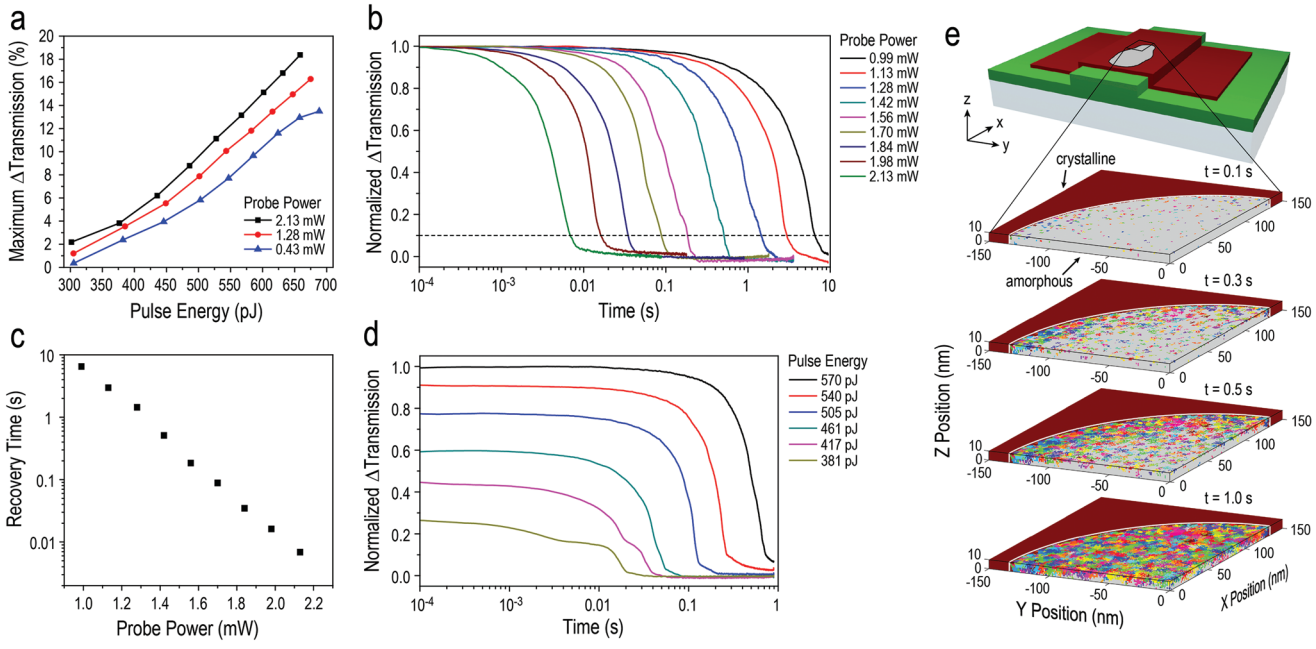

Figure 2. Recrystallization dynamics of volatile memory. a) Maximum change in transmission as a function of WRITE pulse energy for three different probe powers. Increasing the probe power increases the absorption of the WRITE pulse which is able to switch more material to the amorphous state. b) Normalized change in transmission for a fixed energy WRITE pulse (485 pJ) and various probe powers. The retention time of the material decreases with increasing probe power. c) Recovery time (time required for transmission to recover to 10% of maximum ΔT) as a function of probe power as observed from data in inset (b). d) Normalized change in transmission for a fixed probe power and various WRITE pulse energies. Lower energy WRITE pulses only partially amorphize the GST, leading to higher optical absorption and shorter recovery times. e) Simulation of the optically induced recrystallization dynamics after the initial WRITE pulse. Recrystallization is mainly by nucleation (due to the relatively low temperatures induced by the probe), and the nucleation rate is the highest at the edge of the amorphous mark (due to the significantly higher absorption of the background crystalline phase).

device at various probe powers during the recrystallization process. After the initial WRITE pulse at 0 s, a region of the GST is in the amorphous state, ΔT is maximum, and the absorption of the probe is reduced. However, a portion of the optical probe is still absorbed by the remaining crystalline region of the GST which heats the material and causes crystallization to occur at a rate dependent on the material temperature.[37,38]

A clear trend is observed in the recovery time of the material which we have defined as the amount of time required for ΔT to equal 10% of ΔT_{max} (see dashed line in Figure 2b). We have plotted the recovery time as a function of probe power in Figure 2c and observe an exponential dependence. Our results show that optical control of the data retention time, i.e., volatility control, can be achieved over more than six orders of magnitude (see Section S1 in the Supporting Information for retention times greater than 10 s). This ability to tune our device's retention time over such a wide range of recovery times broadens its usefulness for various applications, including neuromorphic computing, reservoir computing, and coincidence detection (as discussed in the "Introduction").

To determine the influence of the WRITE pulse on the recovery time of our device, we kept the probe power fixed at 1.70 mW and varied the WRITE pulse energy (Figure 2d). One can see that both the maximum transmission and recovery time decrease with decreasing WRITE pulse energy. This is easily explained by the difference in optical absorption for a device with a small versus large amorphous region. The lower the WRITE pulse energy, the greater the fraction of GST remaining in the crystalline state, leading to more absorption of the probe which increases the GST temperature and causes a faster recovery time.

To better understand the recrystallization process in our device, we developed a simulation framework by which we could account for time-varying optical, thermal, and crystallization growth dynamics simultaneously. Since the temperature influences both the complex refractive index and rate of recrystallization in GST, which in turn effects the optical absorption and temperature of the device, it is crucial to use a time-dependent, iterative model (Section S3 in the Supporting Information). In our simulations, we initialize a fixed amorphous region and monitor the crystal growth for different probe powers. Figure 2e shows a partial cross section of the GST volume at four different instances in time for a fixed 1.28 mW optical probe, showing that the crystal growth begins at the amorphous–crystalline interface where the temperature of the amorphous region is greatest.

The ability to operate our device in a volatile manner allows us to perform coincidence detection using the nonlinear nature of GST's phase-change transition. As pointed out in the introductory section, coincidence detection has important applications in neuromorphic computing based on the spatiotemporal structure of neuron spiking patterns,[24] the training of neural networks[25] and machine learning.[26] In order to switch GST from a crystalline to an amorphous state, a certain threshold temperature must be reached. We set the optical power of the WRITE pulses such that a single pulse will heat the GST below this switching threshold, but two overlapping pulses will surpass this threshold as illustrated in **Figure 3**a. Therefore, the optical transmission

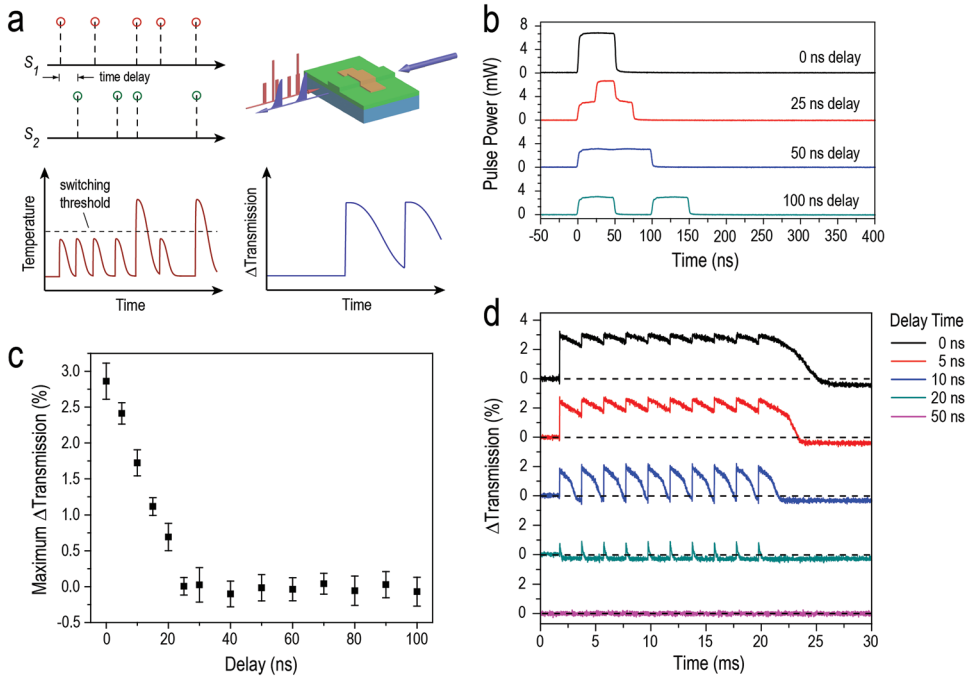

Figure 3. Detecting coincident events between two signals using volatile phase-change memory. a) Illustration of binary coincidence detection using GST in volatile operation. Only when two pulses overlap in time will the combined optical power surpass the threshold required to reach an amorphous state (higher transmission level). An optical probe recrystallizes the GST which "resets" the device to detect the next event. b) Total optical power of two WRITE pulses with four different time delays measured with a fast photodetector. Peak power varies with delay, but total energy remains constant. c) Maximum change in transmission for two 50 ns WRITE pulses with varying time delays. At 0 ns time delay, the transmission reaches a maximum indicating the two pulses are correlated in time. d) Multipulse device dynamics using two pulse trains with varying time delays between them. When the two pulse trains are overlapped in time, the transmission is at a maximum, indicating the two signals are correlated.

will change only when two WRITE pulses overlap in time. Figure 3b shows the measured optical power of four sets of these pulses with different time delays. In Figure 3c we plot the peak response of our device for a high-power probe when two 50 ns WRITE pulses separated by various time delays are coincident at the device. If we integrate the optical power in Figure 3b, we see that regardless of the time delay between the two WRITE pulses, the total energy remains constant at $E_{\text{pulses}} = 340 \pm 17$ pJ, but the total peak power varies with the time delay. The nonlinear response of GST allows us to determine whether two WRITE pulses overlap in time by observing the device's transmission as shown in Figure 3c. It is worth noting that although the response time of our device is long compared with the time scale of the WRITE pulses (tens of milliseconds versus tens of nanoseconds), we are still able to clearly resolve a 5 ns difference in time delay between two WRITE pulses due to the high speed melting process by which GST reaches an amorphous state. In practice, the accuracy of this technique is largely dependent on the bandwidth and SNR of the photodetector used.

To demonstrate the temporal response of our coincident detector, we performed an additional experiment using signals consisting of multiple pulses. Here, we vary the delay between two identical pulse trains of ten 50 ns WRITE pulses with a 500 Hz repetition rate (Figure 3d). Although in practice the repetition rate could be much higher (limited experimentally to less than 20 MHz by our 50 ns WRITE pulse width), it is instructive to see the response of our device between individual WRITE pulses in the pulse train. At 0 ns time delay, the transmission remains almost constant throughout the duration of the pulse train with small visible spikes in the transmission where the overlapping WRITE pulses occur. As the time delay between the two pulse trains increases, the amplitude and duration of the transmission spikes decrease until they are no longer overlapping. As the time delay increases further, the transmission response disappears indicating the two pulse trains are no longer correlated in time.

In a final experiment, we examine the volatile response of a 0.5 μm strip of GST placed on a ring resonator coupled to two bus waveguides (see **Figure 4**a). In this configuration, five 1.5 ps WRITE pulses separated by 25 ns are coupled to the add port of the resonator while the optical probe is on resonance with the cavity (1557 nm) is coupled to the opposite input port. When the GST is in the crystalline state, the probe is undercoupled to the ring which results in a higher output power at the through port than the drop port as shown in Figure 4b. After sending a train of five WRITE pulses to the ring (total energy of 50.5 pJ and centered at 1565 nm), the GST is in the amorphous state and optical power from the probe is coupled to the drop port. This provides an all-optical framework for routing light based on the state of the GST and has been demonstrated as a nonvolatile 1×2 all-optical switch[39] and recently proposed as a method for implementing an all-optical phase change spiking neuron.[40] In the latter case, however, the use of a nonvolatile PCM requires additional logic to reset the device once threshold is reached. By combining the artificial volatility we observe in GST with such a photonic spiking neural network, it could be possible to achieve optically tunable "leaky integrate and fire" functionality without any added complexity to the photonic architecture proposed by Chakraborty et al.[40]

From the perspective of volatility, integrating GST in an optical resonator has the added benefit of lowering the probe power required for initiating volatility in addition to providing greater contrast between two transmission states. In Figure 4c, we show that the probe power required to recrystallize the GST is reduced by approximately a factor of four compared to the GST on the waveguide (see Figure 2b). Here, we fix the WRITE pulse energy at 41.1 pJ and vary the probe power while monitoring the drop and through ports. As discussed previously, higher probe powers increase the material absorption and cause the WRITE pulses to amorphize a larger area of the GST resulting in an increased maximum switching contrast. The ring also has the added benefit of increasing the contrast between the amorphous and crystalline states, which is double that of the 2 μm long GST (compare Figures 4d and 2a). This can be attributed both to the smaller area of GST (0.5×0.75 μm^2 versus 2×1.3 μm^2) and field enhancement of the ring itself. While these results are beneficial for applications requiring volatility, we note that for nonvolatile applications, such as optical routing[39] or multiplexed photonic memory,[10] one must be aware that optical power in the resonator can have this volatile effect on optical PCMs.

In Figure 4d, we fix the probe power at 640 μW (measured in the bus waveguide, after the input grating coupler) while varying the energy of the WRITE pulses. Higher switching contrast again reduces the speed of recrystallization due to lower absorption of the probe. Previous work in a similar (but nonvolatile) device measured the switching speed of GST amorphization to be on the order of 200 ps while recrystallization required a train of ≈600 pulses with decreasing amplitude.[39] This method, similar to previous techniques,[10,17,41] requires multiple pulses to fully reach crystallization with speeds ranging from several to tens of microseconds. Here, we maintain sub-nanoseconds amorphization switching speeds as with previous results, but sacrifice some speed during the recrystallization process (maximum recrystallization time of 850 μs in Figure 4c) in favor of much simpler control over the data retention time in our device. Additionally, the rich time-dependent dynamics observed in Figure 4c,d are not observed with nonvolatile switching methods. While these results already show significant improvement over the device used in Figures 1–3 in terms of contrast, speed, and energy efficiency, further optimization in the coupling between the bus waveguides and ring resonator to better match the loss of the GST (i.e., "critical coupling") could provide much greater gains.

3. Conclusion

In conclusion, we have observed volatile behavior in a traditionally nonvolatile PCM, demonstrating that the best of both worlds can be attained with a single material. By varying the optical power of the probe, we observed an exponential decrease in the data retention time of our PCM memory cell, enabling retention times ranging from years (nonvolatile operation) to milliseconds (volatile operation). Crucially, by developing an advanced multiphysics model, we show that the recrystallization dynamics of the materials at higher probe powers

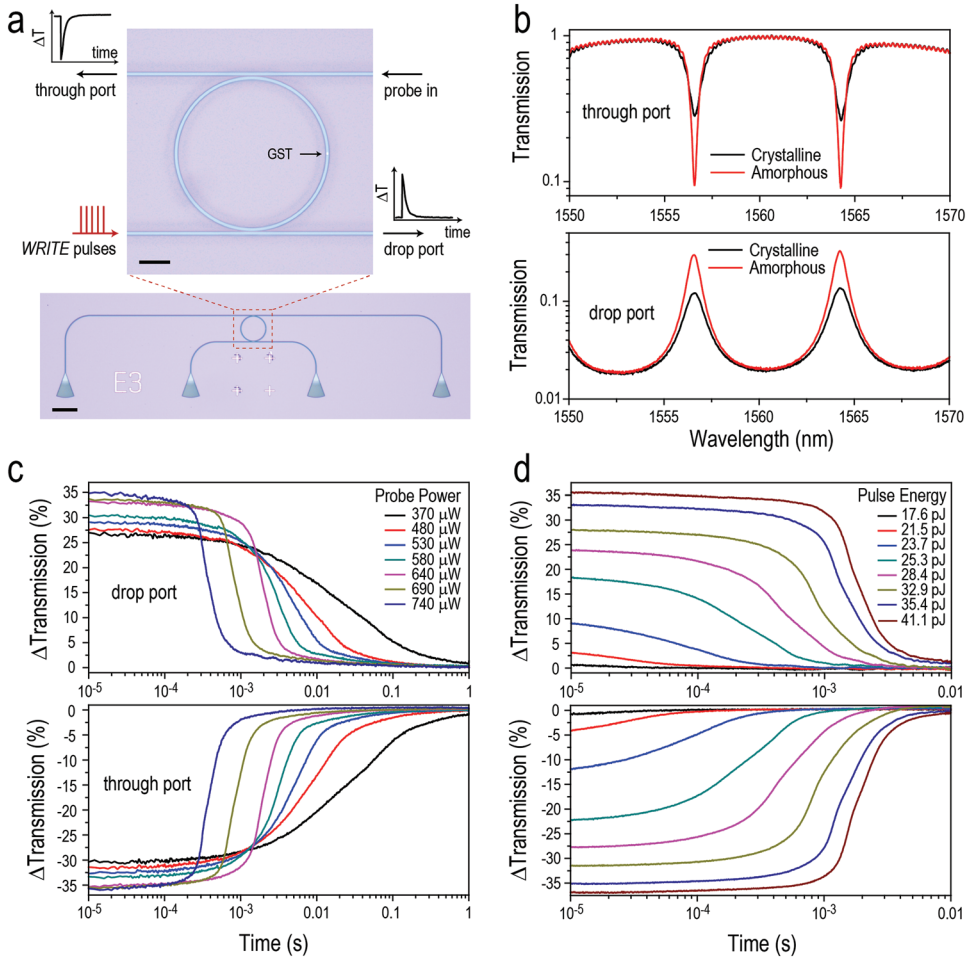

Figure 4. Improved efficiency and switching contrast using a photonic ring resonator. a) A 0.5 μm GST strip is placed on a ring resonator which is coupled to two bus waveguides (Scale bars are 10 and 50 μm for the ring resonator and full device images respectively). The optical probe is routed to the drop port from the through port when the GST is in the amorphous state. b) Spectrum of the resonator when GST is in the amorphous and crystalline states. c) Recrystallization dynamics for a fixed pulse energy (41.1 pJ) and varying probe power. Increased transmission is observed at high probe powers due to increased absorption. d) Pulse energy dependent recrystallization for a fixed probe power (640 μW). The pulse energy is reduced by an order of magnitude from the device in Figure 2 due to the reduced size of the GST and the use of picosecond WRITE pulses.

determine its volatility, and therefore can be controlled at will. This was achieved in a fully integrated and optical platform and used for both multilevel data storage and detecting coincident events between two binary signals. By operating our device in a volatile manner, we were able to resolve timing differences as low as 5 ns between two pulses. Further experiments showed similar behavior between two trains of multiple pulses, indicating volatile phase-change photonics could be used to detect coincident events between two optical signals. We also reduced the power and speed requirements for both recrystallization and optical switching by an order of magnitude by integrating GST in a ring resonator. This design enables greater switching contrast and the ability to route light from one waveguide to another with an intrinsically controllable "reset" via volatility and features rich, time-dependent optical dynamics. Our results demonstrate that phase-change photonics utilizing nonvolatile elements can also be configured as volatile elements and thus provide a promising platform for all-optical data storage and computation.

4. Experimental Section

Sample Fabrication: The devices were fabricated using wafers coated with 330 nm Si_3N_4 on 2 μm buried oxide. Electron-beam lithography (EBL) was used to define the photonics layer and grating couplers with maN-2403 resist and a subsequent RIE etch step. The sample was then coated with poly(methyl methacrylate) (PMMA) and aligned EBL was used to open windows for GST deposition. A 10 nm GST and 10 nm ITO capping layer were deposited using RF sputtering with an argon plasma (70 sccm Ar, RF power 30 W, and base pressure 2×10^{-7} Torr). The PMMA and unwanted sputtered material were then removed using a lift-off process. A 10 min anneal at 250 °C on a hot plate crystallized the GST and increased optical absorption for subsequent optical measurements.

Measurement Setup: A fiber array containing multiple single mode fibers was used to couple light from 1598 nm WRITE pulse and 1590 nm probe lasers into our devices via on-chip grating couplers. 50 ns pump pulses were generated using a CW seed laser modulated by an electro-optic modulator (Lucent EOM) and amplified using an L-band erbium doped fiber amplifier (EDFA). The WRITE pulse and probe were coupled into and out of our device by opposite grating couplers such that the WRITE pulse and probe were counter propagating in our device. The resulting output WRITE and probe powers were monitored by a 1 GHz

low noise photodetector (Newport 1611) and a DC to 125 MHz low noise photodetector (Newport 1811) respectively. Optical tunable bandpass filters (Santec OTF-320) were used to isolate the WRITE and probe signals before encountering the photodetectors. For ring resonator measurements, a 40 MHz mode-locked femtosecond fiber laser (Pritel, FFT) with 1.5 ps pulse width and centered at 1565 nm was used switch the GST. Pulse trains of five pulses with 25 ns spacing were selected with a homemade pulse picker, acousto-optic modulator, and 500 MHz pulse generator. Further amplification of the pulses was achieved with an erbium-doped fiber amplifier (Pritel, LNHPFA-33).

Supporting Information

Supporting Information is available from the Wiley Online Library or from the author.

Acknowledgements

This research was supported by EPSRC via grants EP/J018694/1, EP/M015173/1, and EP/M015130/1 in the UK; the Deutsche Forschungsgemeinschaft (DFG) grant PE 1832/2-1 in Germany; the European Research Council grant 682675; and from the European Union's Horizon 2020 research and innovation programme under grant agreement No 780848 (Fun-COMP project). H.B. thanks A. Ne for stimulating conversations. All authors thank the collaborative nature of European science for allowing this work to be carried out.

Conflict of Interest

Several authors have filed patent applications in the field of photonic memory and computing including in the use of tunable volatility.

Keywords

all-optical computing, integrated all-photonic memory, phase-change materials, phase-change photonics

Received: October 26, 2018
Revised: January 6, 2019
Published online:

[1] N. Yamada, E. Ohno, K. Nishiuchi, N. Akahira, M. Takao, *J. Appl. Phys.* **1991**, *69*, 2849.
[2] M. Wuttig, N. Yamada, *Nat. Mater.* **2007**, *6*, 824.
[3] P. Hosseini, C. D. Wright, H. Bhaskaran, *Nature* **2014**, *511*, 206.
[4] C. Ríos, P. Hosseini, R. A. Taylor, H. Bhaskaran, *Adv. Mater.* **2016**, *28*, 4720.
[5] B. Broughton, L. Bandhu, C. Talagrand, S. Garcia-Castillo, M. Yang, H. Bhaskaran, P. Hosseini, *SID Symp. Dig. Tech. Pap.* **2017**, *48*, 546.
[6] T. Cao, C. Wei, R. E. Simpson, L. Zhang, M. J. Cryan, *Sci. Rep.* **2015**, *4*, 3955.
[7] B. Gholipour, J. Zhang, K. F. MacDonald, D. W. Hewak, N. I. Zheludev, *Adv. Mater.* **2013**, *25*, 3050.
[8] Q. Wang, E. T. F. Rogers, B. Gholipour, C.-M. Wang, G. Yuan, J. Teng, N. I. Zheludev, *Nat. Photonics* **2016**, *10*, 60.
[9] C. Rios, P. Hosseini, C. D. Wright, H. Bhaskaran, W. H. P. Pernice, *Adv. Mater.* **2014**, *26*, 1372.
[10] C. Ríos, M. Stegmaier, P. Hosseini, D. Wang, T. Scherer, C. D. Wright, H. Bhaskaran, W. H. P. Pernice, *Nat. Photonics* **2015**, *9*, 725.
[11] A. Pirovano, A. L. Lacaita, A. Benvenuti, F. Pellizzer, R. Bez, *IEEE Trans. Electron Devices* **2004**, *51*, 452.
[12] S. Raoux, G. W. Burr, M. J. Breitwisch, C. T. Rettner, Y.-C. Chen, R. M. Shelby, M. Salinga, D. Krebs, S.-H. Chen, H.-L. Lung, C. H. Lam, *IBM J. Res. Dev.* **2008**, *52*, 465.
[13] S.-H. Lee, Y. Jung, R. Agarwal, *Nat. Nanotechnol.* **2007**, *2*, 626.
[14] T. V. P. Bliss, G. L. Collingridge, *Nature* **1993**, *361*, 31.
[15] H. Markram, Y. Wang, M. Tsodyks, *Proc. Natl. Acad. Sci. USA* **1998**, *95*, 5323.
[16] S. J. Martin, P. D. Grimwood, R. G. M. Morris, *Annu. Rev. Neurosci.* **2000**, *23*, 649.
[17] Z. Cheng, C. Ríos, W. H. P. Pernice, C. D. Wright, H. Bhaskaran, *Sci. Adv.* **2017**, *2*, 1.
[18] A. N. Burkitt, *Biol. Cybern.* **2006**, *95*, 1.
[19] R. B. Stein, *Biophys. J.* **1965**, *5*, 173.
[20] B. Schrauwen, D. Verstraeten, J. Van Campenhout, *Proc. 15th Eur. Symp. Artif. Neural Networks* **2007**, pp. 471–482, http://dx.doi.org/1854/11063.
[21] D. Verstraeten, B. Schrauwen, D. Stroobandt, in *The 2006 IEEE Int. Joint Conf. Neural Network Proc.*, IEEE, Vancouver, BC, **2006**, pp. 1050–1053, http://dx.doi.10.1109/IJCNN.2006.246804.
[22] P. Joshi, W. Maass, presented at *Biologically Inspired Approaches to Advanced Information Technology*, Switzerland, January **2004**.
[23] M. Oubbati, M. Schanz, T. Buchheim, P. Levi, presented at *RoboCup 2006: Robot Soccer World Cup X*, Germany, June **2006**, pp. 691–701.
[24] R. Gütig, H. Sompolinsky, *Nat. Neurosci.* **2006**, *9*, 420.
[25] S. E. Fahlman, C. Lebiere, in *Advances in Neural Information Processing Systems 2*, (Ed: D. S. Touretzky), **1990**, pp. 524–532.
[26] A. Sebastian, T. Tuma, N. Papandreou, M. Le Gallo, L. Kull, T. Parnell, E. Eleftheriou, *Nat. Commun.* **2017**, *8*, 1115.
[27] K. Bergman, J. Shalf, T. Hausken, *Opt. Photonics News* **2016**, *27*, 32.
[28] R. M. Briggs, I. M. Pryce, H. A. Atwater, *Opt. Express* **2010**, *18*, 11192.
[29] J. D. Ryckman, K. A. Hallman, R. E. Marvel, R. F. Haglund, S. M. Weiss, *Opt. Express* **2013**, *21*, 10753.
[30] G. Kaplan, K. Aydin, J. Scheuer, *Opt. Mater. Express* **2015**, *5*, 2513.
[31] O. L. Muskens, L. Bergamini, Y. Wang, J. M. Gaskell, N. Zabala, C. de Groot, D. W. Sheel, J. Aizpurua, *Light: Sci. Appl.* **2016**, *5*, e16173.
[32] Y. Abate, R. E. Marvel, J. I. Ziegler, S. Gamage, M. H. Javani, M. I. Stockman, R. F. Haglund, *Sci. Rep.* **2015**, *5*, 13997.
[33] R. Bruck, K. Vynck, P. Lalanne, B. Mills, D. J. Thomson, G. Z. Mashanovich, G. T. Reed, O. L. Muskens, *Optica* **2016**, *3*, 396.
[34] A. V. Kolobov, P. Fons, A. I. Frenkel, A. L. Ankudinov, J. Tominaga, T. Uruga, *Nat. Mater.* **2004**, *3*, 703.
[35] M. Stegmaier, C. Ríos, H. Bhaskaran, W. H. P. Pernice, *ACS Photonics* **2016**, *3*, 828.
[36] L. Waldecker, T. A. Miller, M. Rudé, R. Bertoni, J. Osmond, V. Pruneri, R. E. Simpson, R. Ernstorfer, S. Wall, *Nat. Mater.* **2015**, *14*, 991.
[37] A. Sebastian, M. Le Gallo, D. Krebs, *Nat. Commun.* **2014**, *5*, 4314.
[38] M. Salinga, E. Carria, A. Kaldenbach, M. Bornhöfft, J. Benke, J. Mayer, M. Wuttig, *Nat. Commun.* **2013**, *4*, 2371.
[39] M. Stegmaier, C. Ríos, H. Bhaskaran, C. D. Wright, W. H. P. Pernice, *Adv. Opt. Mater.* **2017**, *5*, 1600346.
[40] I. Chakraborty, G. Saha, A. Sengupta, K. Roy, *Sci. Rep.* **2018**, *8*, 12980.
[41] J. Feldmann, M. Stegmaier, N. Gruhler, C. Ríos, H. Bhaskaran, C. D. Wright, W. H. P. Pernice, *Nat. Commun.* **2017**, *8*, 1256.